Letter

Detecting Majorana modes by readout of poisoning-induced parity flips

Jens Schulenborg,[1] Svend Krøjer,[1] Michele Burrello,[1,2] Martin Leijnse,[3,1] and Karsten Flensberg[1]
[1]*Center for Quantum Devices, Niels Bohr Institute, University of Copenhagen, DK-2100 Copenhagen, Denmark*
[2]*Niels Bohr International Academy, Niels Bohr Institute, University of Copenhagen, DK-2100 Copenhagen, Denmark*
[3]*Solid State Physics and NanoLund, Lund University, Box 118, S-221 00 Lund, Sweden*

(Received 19 September 2022; accepted 17 February 2023; published 3 March 2023)

Reading out the parity degree of freedom of Majorana bound states is key to demonstrating their non-Abelian exchange properties. Here, we present a low-energy model describing localized edge states in a two-arm device. We study parity-to-charge conversion based on coupling the superconductor bound states to a quantum dot whose charge is read out by a sensor. The dynamics of the system, including the readout device, is analyzed in full using a quantum-jump approach. We show how the resulting signal and signal-to-noise ratio differentiates between local Majorana and Andreev bound states.

DOI: 10.1103/PhysRevB.107.L121401

Topological superconductors host Majorana zero-energy modes [1,2] that store quantum information nonlocally, and are thereby in principle protected against local perturbations. Many protocols to detect this nonlocal storage have been theorized in fractional quantum Hall systems [3] and, more recently, in superconducting wires [4–12]. The latter are inspired by the idea of engineered topological superconductors, many of which have been realized experimentally. Transport spectroscopy and interference [13–19] indeed suggests the presence of Majoranas in such systems, but differentiating between topological and trivial states remains challenging [20–27]. Most importantly, however, transport via the states of interest themselves *violates the conservation of fermionic parity* essential to most topological qubit proposals.

The key question addressed in this Letter is thus how to test for Majoranas directly via the conserved parity of nonlocal Majorana pairs, using the same readout device as in the intended quantum information application. Typical parity measurement schemes are theorized to rely on a conversion to a charge or magnetic flux when the Majorana modes overlap [4,6,8–11,28–37]. Here, we consider parity-to-charge conversion with a quantum dot coupled to the subgap end states of superconducting wires, such that the dot charge measures the combined dot-subgap parity [6,10,11,35,36,38]. Integrating dots into semiconductor-superconductor structures is experimentally well developed [39–46]: Couplings are accurately tuned via gate voltages, and charge readout is performed via electromagnetic resonators [47–55], sensor dots [56–62], or quantum point contacts [63–67].

However, while the parity-to-charge conversion principle is well established, its implementation raises many fundamental questions which we answer in this Letter. First, can the charge detection, even in principle, differentiate Majorana modes from Andreev bound states? Second, do readout fluctuations provide additional information about these modes? And third, how do the coupling strengths affect the detection scheme?

We concretely study the system in Fig. 1(a): Two superconducting wires with one or several subgap states at their ends (black dots) are tunnel-coupled to a parity-to-charge converter dot (CD). The stable charge of this dot changes with subgap parity flips [6], which we assume to be simply due to rare but inevitable quasiparticle (QP) poisoning [68–73] on a timescale t_{QP}. As the occasional CD charge jumps affect a capacitively coupled sensor dot (SD), the parity flips are measurable via telegraph noise in the zero-bias SD conductance G across two tunnel-coupled leads [Fig. 1(b)]. We calculate this conductance by explicitly mimicking the experimental lock-in charge readout technique [56,74]: Applying a small ac voltage

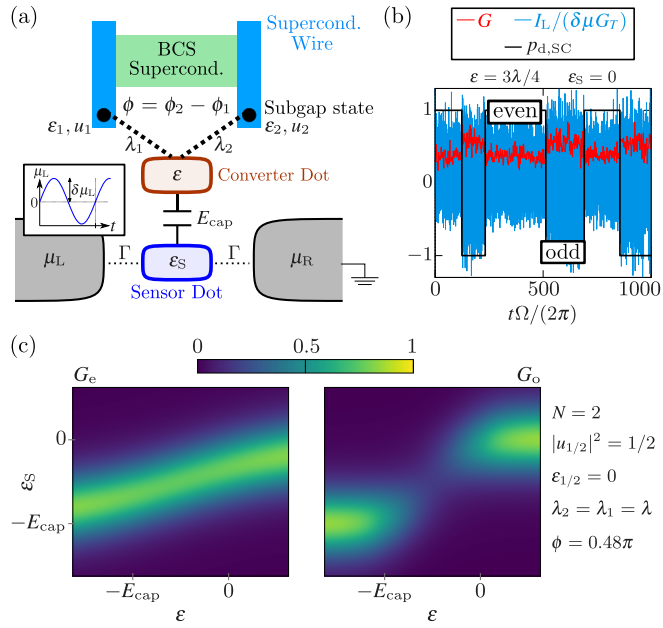

FIG. 1. (a) Subgap modes in two superconducting wires tunnel-coupled to a parity-to-charge converter dot [Eq. (1)] that capacitively couples to a charge sensor. (b) Sensor current $I_{\mathrm{L}}(t)$ due to driven μ_{L}, corresponding first harmonic $G(t)$ [Eq. (2)], and dot-subgap parity $p_{\mathrm{d,SC}}$. (c) Sample-averaged conductances $G_{\mathrm{e/o}} = G_{p_{\mathrm{d,SC}}=\pm 1}$ scaled by $G_T = \Gamma/(8T)$. (b) shares parameters with (c); other parameters are from Fig. 2.

at zero dc bias, the equal-frequency first harmonic current response provides a measure for G. The strength and unique feature of our approach is to quantify the conductance as directly sampled from the experimentally accessible readout signal $G(t)$, including SD backaction via a consistent quantum master equation [35,38,75,76] in a quantum-jump Monte Carlo simulation [77–80]. We thereby capture the effect of measurement-induced relaxation, thermal- and nonequilibrium noise, and of the lock-in drive as well as the readout integration time. This includes possible signal loss due to state projections away from the CD-subgap ground state [6,35,36,81].

The low-energy Hamiltonian for the single-level CD with energy ϵ, N superconducting subgap modes i at energies ϵ_i in either wire, and the CD-subgap tunnel couplings $\lambda_{i=1,\ldots,N}$ read ($|e| = \hbar = k_B = 1$)

$$H_{\mathrm{d,SC}} = \epsilon n + \sum_{i=1}^{N} \epsilon_i n_i + \sum_{i=1}^{N} \lambda_i e^{i\phi_i} d^\dagger [|u_i|\alpha_i + |v_i|\alpha_i^\dagger] + \mathrm{H.c.} \tag{1}$$

Here, $n = d^\dagger d$ is the CD occupation with fermionic creation/annihilation operator $d^\dagger, d$; the subgap state occupations $n_i = \alpha_i^\dagger \alpha_i$ are likewise associated with the creation/annihilation operators $\alpha_i^\dagger, \alpha_i$. To justify the single-level dot picture, we assume both the CD single-particle level spacing and on-site Coulomb interaction to be large compared to the tunneling amplitudes λ_i [38]. This implies sufficient CD-spin polarization, motivated by the large magnetic field needed for Majorana modes [82,83]. We, however, allow for subgap modes with $\epsilon_i \neq 0$, with spin-axis orientations different from the CD [84,85], and with (normalized, $|u_i|^2 + |v_i|^2 = 1$) couplings featuring unequal particle and hole components $|u_i| \neq |v_i|$ and mode-dependent phases $\phi_i \neq \phi_j$. Unlike previous works [6,10,35,36,38] which assumed a dot coupling to only one Majorana per wire, we thus represent $H_{\mathrm{d,SC}}$ in terms of fermionic fields $\alpha_i^\dagger, \alpha_i$ instead of Majorana operators. These fermions are gauged to obtain $\lambda_i \geqslant 0$, so phases enter Eq. (1) exclusively via $e^{i\phi_i}$. These depend on uncontrollable CD/subgap wave function details, but in the important case of one fermion per wire, the only relevant phase difference $\phi_2 - \phi_1 = \phi$ is flux (ϕ) tunable.

The model (1) implies quantum fluctuations in all occupations n, n_i and their sum $n_{\mathrm{d,SC}} = n + \sum_{i=1}^{N} n_i$, but leaves the combined parity $p_{\mathrm{d,SC}} = (-\mathbb{1})^{n_{\mathrm{d,SC}}}$ a good quantum number. Our central question is how this parity $p_{\mathrm{d,SC}}$—converted to the CD charge ($\langle n \rangle$) affecting the SD conductance [Figs. 1(a) and 1(b)]—distinguishes between finite- and zero-energy Andreev and Majorana wire modes. The capacitive coupling $H_{\mathrm{cap}} = E_{\mathrm{cap}} n_S n$ to the SD charge n_S is quantified by E_{cap}. The SD tunnel-couples to metallic noninteracting leads, assuming symmetric, energy-independent tunneling rates $\Gamma_{L/R} = \Gamma$ [80,86]. The Supplemental Material [80] details how we obtain the time-resolved conductance from the quantum-jump method [77–79], with universal Lindblad operators [35,38,75,76] applicable even for the here relevant near-degenerate states. We assume weak coupling compared to the lead temperature, $\Gamma \ll T$, and lead-internal relaxation as the shortest timescale in the problem.

In brief, our method yields current-time series admitting sample averaging. After each numerical time step $\delta t \ll \Gamma^{-1}$ of each series, we record the accumulated number of electron jumps $J_{r\eta}(t)$ to ($\eta = +$) and from ($\eta = -$) lead r, and calculate the current $I_L(t) = \sum_{\eta=\pm} (\eta/t_b)[J_{L\eta}(t) - J_{L\eta}(t - t_b)]$ with the bandwidth $(1/t_b) < \Gamma$ reflecting detector-internal time averaging. Mimicking the experimental lock-in technique, the zero-bias conductance signal $G(t)$ is extracted from $I_L(t)$ by applying a low-amplitude voltage oscillation $\mu_L(t) = \mu_R + \delta\mu \sin(\Omega t)$ with frequency $(1/t_{QP}) \ll \Omega \ll (1/t_b)$, and by taking the first harmonic response divided by $\delta\mu \lesssim T$. Explicitly, each $G(t)$ sample averages over N_{osc} voltage oscillations,

$$G(t) = \frac{\Omega \delta t / G_T}{\pi N_{\mathrm{osc}} \delta\mu} \left| \sum_{n=0}^{\lceil \frac{2\pi N_{\mathrm{osc}}}{\Omega \delta t} \rceil - 1} I_L(t + n\delta t) e^{-in\Omega\delta t} \right|, \tag{2}$$

where $G_T = \Gamma/(8T)$ is the spinless on-resonance conductance [86]. Figure 1(b) shows the difference between the raw conductance time series $I_L(t)/(\delta\mu G_T)$ and the first harmonic response. The sudden jumps causing the telegraph noise stem from randomly inserted $p_{\mathrm{d,SC}}$ flips [68–73]. Just as in experiments, $G(t)$ filters out high frequencies via the Fourier transform, bounding the noise spectrum not by the inaccessible bandwidth $1/t_b$, but by the well-controlled lock-in frequency Ω.

The even/odd-parity conductances $G_{e/o} = \langle G \rangle_{M, p_{\mathrm{d,SC}} = \pm 1}$ in Fig. 1(c) are averages over $M = N_T M_T$ samples from N_T trajectories $G(t)$ *at fixed* $p_{\mathrm{d,SC}} = \pm 1$; each trajectory consists of M_T subsequent samples in a time $\Delta t = M_T N_{\mathrm{osc}} \frac{2\pi}{\Omega} \leqslant t_{QP}$ expected to be within two QP poisonings [80], as exemplified by the typical G-plateau length in Fig. 1(b). The $G_{e/o}$ and their fluctuations $\delta G_{e/o} = \sqrt{\langle G^2 \rangle_{M, p_{\mathrm{d,SC}} = \pm 1} - G_{e/o}^2}$ define the signal $\mathcal{S}$ and signal-to-noise ratio (SNR) $\mathcal{D}$:

$$\mathcal{S} = |G_e - G_o|, \quad \mathcal{D} = 2\mathcal{S}/(\delta G_e + \delta G_o). \tag{3}$$

The ratio $\mathcal{D}$ as a function of the tunable CD level ϵ and flux ϕ is our key observable to characterize the subgap states, as it sets the number of G samples required for statistically significant parity distinguishability. We, however, also refer to $\mathcal{S}$, mostly based on data in the Supplemental Material [80], to rule out or identify any nontrivial scaling between noise and signal. This furthermore allows us to estimate how the distinguishability would diminish with additional noise unaccounted for here.

The detector setup and SD level ϵ_S for optimal $\mathcal{D}$ depends on both E_{cap} and λ_i [80], since $\mathcal{S}, \mathcal{D} > 0$ are due to $p_{\mathrm{d,SC}}$-dependent CD-subgap hybridization inducing a $p_{\mathrm{d,SC}}$-dependent conductance peak shift away from the classical resonances $\epsilon_S = 0, -E_{\mathrm{cap}}$. We here focus on $E_{\mathrm{cap}} > \lambda_i$, yielding nearly classical G_o peaks and sizably deviating G_e [Fig. 1(c)]. The largest $\mathcal{S}$ then appears between Coulomb peaks, $\epsilon_S = -E_{\mathrm{cap}}/2$, but this point is often susceptible to the here neglected higher-order-Γ effects such as Kondo resonances. We hence instead fix $\epsilon_S = 0$ and reduce lead-induced broadening by demanding $\Gamma, T \ll E_{\mathrm{cap}}$. Larger $\frac{\Gamma}{T}, \frac{\delta\mu}{T}$ tend to improve $\mathcal{D}$ [80], but we must keep Γ, $\delta\mu$, and especially T smaller than λ_i; otherwise, capacitive backaction may drive

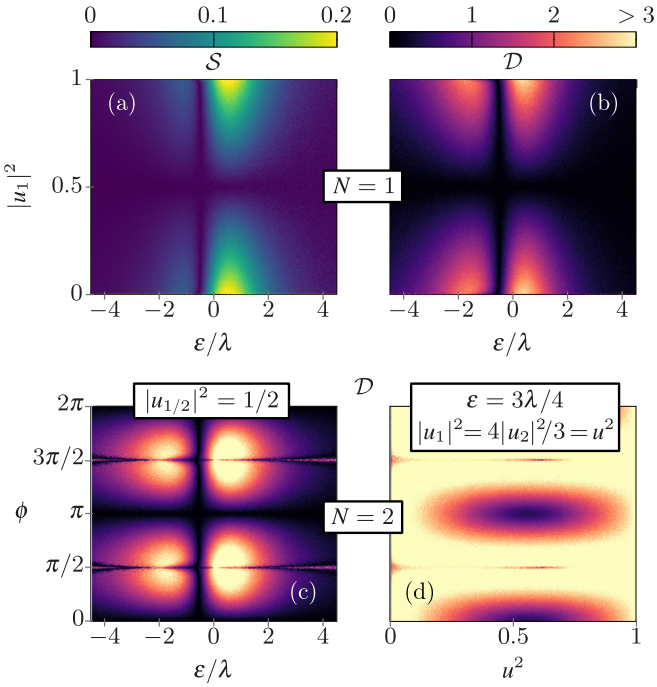

FIG. 2. Signal $\mathcal{S}$ and signal-to-noise ratio $\mathcal{D}$ [Eq. (3)] as a function of various parameters for $N = 1$ [(a), (b)] and $N = 2$ [(c), (d)] zero-energy subgap modes. All panels use $\epsilon_i = 0$, $\lambda_i = \lambda$, $\epsilon_S = 0$, $E_{cap} = 2\lambda = 6T = 6\delta\mu = 20\Gamma$, $2\pi/\Omega = 4t_b = 2\pi \times 2400/\lambda = 10^4\delta t = 1$ μs, $N_{osc} = 2$, $N_T = 10$, $M_T = 50$.

the system too far away from the near-ground state in Fig. 1(c) to obtain a signal [36,38]. Let us now first discuss the ideal limit in Fig. 2, with all subgap energies $\epsilon_i/\lambda_i \to 0$. The CD then effectively couples to only one subgap fermion [80], being a linear combination of all N subgap modes in Eq. (1),

$$H_{d,SC} = \epsilon n + [d^\dagger(\lambda^+\alpha^\dagger + \lambda^-\alpha) + \text{H.c.}], \tag{4}$$

where α is a fermionic annihilation operator and

$$\lambda^\pm = \lambda_{eff}\sqrt{1 \pm \sqrt{1-|\mathcal{Q}|^2}}, \quad \mathcal{Q} = \sum_{i=1}^{N} \frac{\lambda_i^2}{\lambda_{eff}^2} e^{i2\phi_i}|u_i||v_i|, \tag{5}$$

with $0 \leqslant |\mathcal{Q}| \leqslant 1$ and effective coupling $\lambda_{eff} = \sqrt{\sum_{i=1}^{N}\lambda_i^2/2}$. The capacitive readout likewise only senses the subparity of this one α mode and the CD, $p_{d\alpha} = (-\mathbb{1})^{n+\alpha^\dagger\alpha}$; the other $N-1$ orthogonal subgap modes are invisible. For this single remaining mode, $\mathcal{Q}$ generalizes the Majorana quality factor of Refs. [87,88]: Interpolating between a pure particle- or holelike ($|\mathcal{Q}| = 0$), and an equally particle- and holelike coupling ($|\mathcal{Q}| = 1$), the latter crucially maps to the single-Majorana case:

$$H_{d,SC} \overset{|\mathcal{Q}|=1}{\to} \epsilon n + \lambda_{eff}(d^\dagger - d)\gamma, \tag{6}$$

with $\gamma = \alpha^\dagger + \alpha$. The sensor is then insensitive to $p_{d\alpha}$ [6], and yields $\mathcal{S} = \mathcal{D} = 0$ for any ϵ, λ_i within the single-level CD approximation. We emphasize that for this (ϵ, λ_i)-independent parity insensitivity, $\epsilon_i/\lambda_i \to 0$ and $|\mathcal{Q}| = 1$ are not only sufficient, but necessary [80]. Following Eq. (5), this means that all N subgap modes i in Eq. (1) must couple as zero-energy Majoranas to the CD, $|u_i| = |v_i|$, and with equal ϕ_i up to a π shift.

The key Majorana signature deriving from Eq. (6) are constant $\mathcal{S}, \mathcal{D} = 0$ with varying individual conductances $G_{e/o}$ in sweeps of the dot level ϵ and, if possible, the coupling strengths λ_i: Constant $G_{e/o}$ may merely indicate insufficient sensor coupling, and if $\mathcal{S}, \mathcal{D} = 0$ only for specific ϵ, λ_i, one can neither rule out fine tuning unrelated to Majoranas, nor the quasi-Majorana case [24] with a coincidentally uncoupled zero mode. Importantly, such a sweep test is inherently robust to fluctuating $\epsilon, \epsilon_S, \lambda_i$ due to, e.g., $1/f$ noise [89–91], and towards unavoidable coupling asymmetries $\lambda_i \neq \lambda_j$ [80].

Table I lists the subgap mode setups for which the suggested prescription can or cannot yield (ϵ, λ_i)-independent $\mathcal{S}, \mathcal{D} = 0$. The simplest case involves only one wire with only one ($N = 1$) coupled mode (see Refs. [87,88,92,93]). For this ϕ-independent situation, Figs. 2(a) and 2(b) show that all ϵ traces approach $\mathcal{S}, \mathcal{D} = 0$ close to the particle-hole symmetry point $\epsilon = 0$, but only a Majorana [$|u_1|^2 = 0.5 \Rightarrow$ Eq. (6)] yields $\mathcal{S} = \mathcal{D} = 0$ for all ϵ. This robustness is equivalent to the single-site protection in the minimal Kitaev chain [92,93], but using it to identify a Majorana in a single, *actual* wire is difficult. First, it relies on the SNR in the Andreev case $|u_1|^2 \neq 0.5$: The parameters in Fig. 2(b) yield $\mathcal{D} > 1$ if $||u_1|^2 - 0.5| \gtrsim 0.1$, which may improve if ϵ_S, E_{cap}, Γ are optimizable within the stated constraints. But more importantly, convincing evidence would also include tunability towards a control case with $\mathcal{S}, \mathcal{D} > 0$ for some ϵ *at fixed* $\epsilon_1/\lambda_1 \to 0$.

The latter is provided when both wires couple, making $\mathcal{S}, \mathcal{D}$ flux (ϕ) tunable as shown for one mode per arm ($N = 2$) in Figs. 2(c) and 2(d). For Majoranas ($|u_{1/2}|^2 = 0.5$), ϵ-independent $\mathcal{S}, \mathcal{D} = 0$ are seen exclusively at $\phi = 0, \pi$ fulfilling Eq. (6), and $\mathcal{D} \gtrsim 1$ already if ϕ deviates by $\sim\pi/20$ with the detector parameters in Fig. 2(c). Given instead at least one zero-energy Andreev mode ($|u_i|^2 \neq 0.5$), ϵ-independent traces $\mathcal{S}, \mathcal{D} = 0$ cannot be observed for any ϕ, with Fig. 2(d)

TABLE I. Setups that do ("Yes")/do not ("No") admit (ϵ, λ_i)-independent $\mathcal{S}, \mathcal{D} = 0$. "Majorana" means all N modes are Majoranas, $|u_i| = 0.5$. "Andreev" means at least one Andreev mode, $|u_i| \neq 0.5$. "No*": $\mathcal{D} \ll 1$ $\forall\epsilon, \phi$ possible if $\Delta t \gtrsim t_p \sim (\lambda/\epsilon_i)^2$ [Fig. 3(b)].

	$\epsilon_i = 0$ for all i		At least one $\epsilon_i \neq 0$
Subgap mode setup	Majorana	Andreev	Any $\lvert u_i\rvert$
$N = 1$	Yes	No	No
$N = 2$, $\phi_2 - \phi_1 = \phi$	If and only if $\phi = 0, \pi$		
$N \geqslant 2$, $\phi_i \neq \phi_j \bmod \pi$	No		No*
$N \geqslant 2$, $\phi_i = \phi_j \bmod \pi$	Yes		

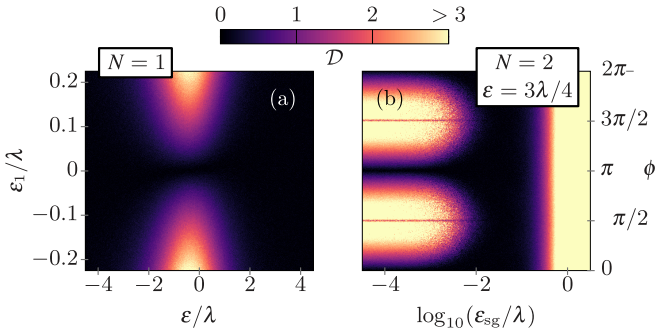

FIG. 3. Signal-to-noise ratio $\mathcal{D}$ [Eq. (3)] as a function of the subgap energies ϵ_i for (a) one coupled wire with $N = 1$, $|u_1|^2 = 0.5$, and (b) one mode per wire, $N = 2$, $|u_i|^2 = 0.5$. In (b), we set $\epsilon_2 = 2\epsilon_1 = 2\epsilon_{sg} > 0$. Other parameters are as in Fig. 2.

exhibiting $\mathcal{D} \geqslant 1$ for $||u_i|^2 - 0.5| \gtrsim 0.1$ close to $\phi = 0, \pi$. A (ϵ, ϕ) profile as in Fig. 2(c) thus strongly indicates Majorana modes in both wires.

Moreover, while the steep ϕ profile increases the susceptibility to flux noise, it also enhances the sensitivity towards additional, typically unwanted zero-energy modes, $N > 2$. This is because even for Majoranas, $|u_i|^2 = 0.5$, the flux cannot generally fix the ϕ_i required for Eq. (6) simultaneously for all $N > 2$ modes. The absence of a line $\mathcal{S}(\epsilon) = \mathcal{D}(\epsilon) = 0$ at a specific flux ϕ then no longer rules out Majoranas (Table I, last two lines), but it remains conclusive in ruling out the Majorana *pair interference* desired for applications in, e.g., qubits.

To finish the analysis in the limit $\epsilon_i/\lambda_i \to 0$, we also highlight the (ϵ, λ_i)-*sensitive* signature at $\phi = \frac{\pi}{2}, \frac{3\pi}{2}$ [Fig. 2(c)], showing reduced $\mathcal{D}$ without $\mathcal{S}$ loss [80] for $|\epsilon| \lesssim \lambda_i$, but enhanced $\mathcal{D}$ at $|\epsilon| \gg \lambda_i$. Here, the particle-hole-mixed subgap modes superpose to a fully electron/holelike effective mode ($\mathcal{Q} = 0$). The CD-subgap tunneling is then nearly blocked for one parity only, $H_{d,SC} \to \epsilon n + \sqrt{2}\lambda_{eff}[d^\dagger \alpha^\dagger + \alpha d]$. The much longer tunneling time for this parity ($p_{d\alpha} = -1$ in our gauge) results in $\mathcal{D}$-lowering noise at fixed $\mathcal{S}$ if the time exceeds the sample time $\sim\Omega^{-1}$, but again raises $\mathcal{S}, \mathcal{D}$ if the hopping time even surpasses the poisoning time t_{QP}. Previous studies of this *parity blockade* focused on one Majorana per wire end [36,38,94]. Our analysis shows blockade for any number $N \geqslant 2$ of Majorana or Andreev modes with $\epsilon_i/\lambda_i \to 0$ [80], but—unlike for Majoranas at $\phi = 0, \pi$—only for specific λ_i permitting $\mathcal{Q} = 0$ in Eq. (5).

The sensor's ability to discern finite subgap energies $\epsilon_i \neq 0$ at specific particle-hole mixing is illustrated in Fig. 3 (Table I, rightmost column). For a single wire ($N = 1$), Fig. 3(a) shows an ϵ regime with $\mathcal{D} \gtrsim 1$ already for small $|\epsilon_1|/\lambda_1 \gtrsim 0.1$ and the given detector parameters, even at $u_1^2 = 0.5$. With $N \geqslant 2$ states in both wires giving rise to ϕ-tunable interference, any $\epsilon_i \neq 0$ now couples the effective mode to the other $N - 1$ formerly invisible subgap modes. The no longer conserved parity $p_{d\alpha}$ then no longer protects against relaxation to an energetically favorable steady state that is independent of $p_{d\alpha}$ right after a QP poisoning. Given a small typical energy difference ϵ_{sg} between effective and orthogonal modes, $0 < \epsilon_{sg}/\lambda \ll 1$ for $\lambda_i \sim \lambda$, and a sensor-dominated dissipation rate $\sim\Gamma$, this relaxation occurs on a timescale $t_p \sim \frac{1}{\Gamma}(\frac{\lambda}{\epsilon_{sg}})^2$. If the trajectory time Δt exceeds t_p, the signal no longer represents the $p_{d\alpha} = \pm 1$ difference. The signal and noise profiles $\mathcal{S}(\epsilon, \phi)$, $\mathcal{D}(\epsilon, \phi)$ may then be suppressed and lose any conclusive feature in a broad parameter range. We exemplify this for one mode per wire in Fig. 3(b), showing the Majorana-specific ϕ profile of Fig. 2(c) to vanish if $t_p(\epsilon_{sg}) \ll \Delta t$. Note that even for weak $\Gamma = \lambda/10$ with typical $\lambda \sim 2.4$ GHz, already $\epsilon_i/\lambda \lesssim 10^{-2}$ leads to rather small $t_p \sim 10$ μs. We furthermore stress that the ϕ variations are significantly attenuated for any ϵ and $|u_i|$ [80], also if $\epsilon_{sg} \gtrsim \lambda$ where $\mathcal{S}, \mathcal{D} \neq 0$. In the latter case, the CD effectively decouples from the wire with the higher-lying level, reducing the problem to the single-wire case in Fig. 3(a).

In conclusion, identifying Majorana modes with a subgap parity readout via a capacitively sensed dot is both a major opportunity and challenge. Table I and Fig. 2(c) show the telltale signature for two topological wires providing a single, nonlocal pair of interfering Majoranas—a level-independent sensor parity signal and signal-to-noise ratio $\mathcal{S}(\epsilon) = \mathcal{D}(\epsilon) = 0$ exclusively at fluxes $\phi = 0, \pi$. This signature is conclusive in that it disappears whenever any Andreev mode, or any additional Majorana orthogonal to the other two Majoranas, couples to the converter dot. Furthermore, our protocol is inherently robust to experimentally unavoidable $1/f$ charge noise and asymmetric wire couplings. A clear inference may, however, still be impeded by flux noise. Moreover, already small subgap mode energies can suppress the ϕ dependence after a perhaps challengingly short decay time t_p. On the flip side, *extracting* t_p by varying measurement times may be an interferometric method to resolve deviations $\epsilon_i \neq 0$ more precisely than dc transport spectroscopy.

We thank Serwan Asaad, Magnus Lykkegaard, Maximilian Nitsch, Felix Passmann, and Charles Marcus for very helpful discussions. The research was supported by the Danish National Research Foundation, the Danish Council for Independent Research Natural Sciences, and the Swedish Research Council (VR). M.B. is supported by the Villum Foundation (Research Grant No. 25310). This work was also funded by the Deutsche Forschungsgemeinschaft (DFG, German Research Foundation) - Project No. 277101999 - CRC 183 and the European Research Council (ERC) under the European Union's Horizon 2020 research and innovation program under Grant Agreement No. 856526.

[1] A. Y. Kitaev, Phys.-Usp. **44**, 131 (2001).
[2] S. Das Sarma, M. Freedman, and C. Nayak, Phys. Rev. Lett. **94**, 166802 (2005).
[3] A. Stern, Ann. Phys. **323**, 204 (2008).
[4] F. Hassler, A. R. Akhmerov, C.-Y. Hou, and C. W. J. Beenakker, New J. Phys. **12**, 125002 (2010).
[5] J. Alicea, Y. Oreg, G. Refael, F. von Oppen, and M. P. A. Fisher, Nat. Phys. **7**, 412 (2011).

[6] K. Flensberg, Phys. Rev. Lett. **106**, 090503 (2011).
[7] F. Hassler, A. R. Akhmerov, and C. W. J. Beenakker, New J. Phys. **13**, 095004 (2011).
[8] T. Hyart, B. van Heck, I. C. Fulga, M. Burrello, A. R. Akhmerov, and C. W. J. Beenakker, Phys. Rev. B **88**, 035121 (2013).
[9] D. Aasen, M. Hell, R. V. Mishmash, A. Higginbotham, J. Danon, M. Leijnse, T. S. Jespersen, J. A. Folk, C. M. Marcus, K. Flensberg, and J. Alicea, Phys. Rev. X **6**, 031016 (2016).
[10] S. Plugge, A. Rasmussen, R. Egger, and K. Flensberg, New J. Phys. **19**, 012001 (2017).
[11] T. Karzig, C. Knapp, R. M. Lutchyn, P. Bonderson, M. B. Hastings, C. Nayak, J. Alicea, K. Flensberg, S. Plugge, Y. Oreg, C. M. Marcus, and M. H. Freedman, Phys. Rev. B **95**, 235305 (2017).
[12] J. Manousakis, A. Altland, D. Bagrets, R. Egger, and Y. Ando, Phys. Rev. B **95**, 165424 (2017).
[13] L. Fu, Phys. Rev. Lett. **104**, 056402 (2010).
[14] M. Hell, K. Flensberg, and M. Leijnse, Phys. Rev. B **97**, 161401(R) (2018).
[15] C. Drukier, H.-G. Zirnstein, B. Rosenow, A. Stern, and Y. Oreg, Phys. Rev. B **98**, 161401(R) (2018).
[16] A. M. Whiticar, A. Fornieri, E. C. T. O'Farrell, A. C. C. Drachmann, T. Wang, C. Thomas, S. Gronin, R. Kallaher, G. C. Gardner, M. J. Manfra, C. M. Marcus, and F. Nichele, Nat. Commun. **11**, 3212 (2020).
[17] D. I. Pikulin, B. van Heck, T. Karzig, E. A. Martinez, B. Nijholt, T. Laeven, G. W. Winkler, J. D. Watson, S. Heedt, M. Temurhan, V. Svidenko, R. M. Lutchyn, M. Thomas, G. de Lange, L. Casparis, and C. Nayak, arXiv:2103.12217.
[18] J. Cayao and A. M. Black-Schaffer, Phys. Rev. B **104**, L020501 (2021).
[19] M. Aghaee, A. Akkala, Z. Alam, R. Ali, A. A. Ramirez, M. Andrzejczuk, A. E. Antipov, P. Aseev, M. Astafev, B. Bauer, J. Becker, S. Boddapati, F. Boekhout, J. Bommer, E. B. Hansen, T. Bosma, L. Bourdet, S. Boutin, P. Caroff, L. Casparis *et al.*, arXiv:2207.02472.
[20] E. Prada, P. San-Jose, and R. Aguado, Phys. Rev. B **86**, 180503(R) (2012).
[21] G. Kells, D. Meidan, and P. W. Brouwer, Phys. Rev. B **86**, 100503(R) (2012).
[22] J. Cayao, E. Prada, P. San-Jose, and R. Aguado, Phys. Rev. B **91**, 024514 (2015).
[23] C. Moore, C. Zeng, T. D. Stanescu, and S. Tewari, Phys. Rev. B **98**, 155314 (2018).
[24] A. Vuik, B. Nijholt, A. Akhmerov, and M. Wimmer, SciPost Phys. **7**, 061 (2019).
[25] H. Pan and S. Das Sarma, Phys. Rev. Res. **2**, 013377 (2020).
[26] R. Hess, H. F. Legg, D. Loss, and J. Klinovaja, Phys. Rev. B **104**, 075405 (2021).
[27] K. Flensberg, F. von Oppen, and A. Stern, Nat. Rev. Mater. **6**, 944 (2021).
[28] C. Ohm and F. Hassler, Phys. Rev. B **91**, 085406 (2015).
[29] K. Gharavi, D. Hoving, and J. Baugh, Phys. Rev. B **94**, 155417 (2016).
[30] C. Malciu, L. Mazza, and C. Mora, Phys. Rev. B **98**, 165426 (2018).
[31] T. Li, W. A. Coish, M. Hell, K. Flensberg, and M. Leijnse, Phys. Rev. B **98**, 205403 (2018).
[32] C. Schrade and L. Fu, Phys. Rev. Lett. **121**, 267002 (2018).
[33] A. L. Grimsmo and T. B. Smith, Phys. Rev. B **99**, 235420 (2019).
[34] G. Széchenyi and A. Pályi, Phys. Rev. B **101**, 235441 (2020).
[35] M. I. K. Munk, J. Schulenborg, R. Egger, and K. Flensberg, Phys. Rev. Res. **2**, 033254 (2020).
[36] J. F. Steiner and F. von Oppen, Phys. Rev. Res. **2**, 033255 (2020).
[37] T. B. Smith, M. C. Cassidy, D. J. Reilly, S. D. Bartlett, and A. L. Grimsmo, PRX Quantum **1**, 020313 (2020).
[38] J. Schulenborg, M. Burrello, M. Leijnse, and K. Flensberg, Phys. Rev. B **103**, 245407 (2021).
[39] L. Hofstetter, S. Csonka, J. Nygård, and C. Schönenberger, Nature (London) **461**, 960 (2009).
[40] S. De Franceschi, L. Kouwenhoven, C. Schönenberger, and W. Wernsdorfer, Nat. Nanotechnol. **5**, 703 (2010).
[41] M. T. Deng, C. L. Yu, G. Y. Huang, M. Larsson, P. Caroff, and H. Q. Xu, Sci. Rep. **4**, 7261 (2014).
[42] M. T. Deng, S. Vaitiekėnas, E. B. Hansen, J. Danon, M. Leijnse, K. Flensberg, J. Nygård, P. Krogstrup, and C. M. Marcus, Science **354**, 1557 (2016).
[43] D. B. Szombati, S. Nadj-Perge, D. Car, S. R. Plissard, E. P. A. M. Bakkers, and L. P. Kouwenhoven, Nat. Phys. **12**, 568 (2016).
[44] M.-T. Deng, S. Vaitiekėnas, E. Prada, P. San-Jose, J. Nygård, P. Krogstrup, R. Aguado, and C. M. Marcus, Phys. Rev. B **98**, 085125 (2018).
[45] J. van Veen, D. de Jong, L. Han, C. Prosko, P. Krogstrup, J. D. Watson, L. P. Kouwenhoven, and W. Pfaff, Phys. Rev. B **100**, 174508 (2019).
[46] D. Razmadze, E. C. T. O'Farrell, P. Krogstrup, and C. M. Marcus, Phys. Rev. Lett. **125**, 116803 (2020).
[47] T. Yoshie, A. Scherer, J. Hendrickson, G. Khitrova, H. M. Gibbs, G. Rupper, C. Ell, O. B. Shchekin, and D. G. Deppe, Nature (London) **432**, 200 (2004).
[48] J. P. Reithmaier, G. Sek, A. Löffler, C. Hofmann, S. Kuhn, S. Reitzenstein, L. V. Keldysh, V. D. Kulakovskii, T. L. Reinecke, and A. Forchel, Nature (London) **432**, 197 (2004).
[49] M. R. Delbecq, V. Schmitt, F. D. Parmentier, N. Roch, J. J. Viennot, G. Fève, B. Huard, C. Mora, A. Cottet, and T. Kontos, Phys. Rev. Lett. **107**, 256804 (2011).
[50] T. Frey, P. J. Leek, M. Beck, A. Blais, T. Ihn, K. Ensslin, and A. Wallraff, Phys. Rev. Lett. **108**, 046807 (2012).
[51] K. D. Petersson, L. W. McFaul, M. D. Schroer, M. Jung, J. M. Taylor, A. A. Houck, and J. R. Petta, Nature (London) **490**, 380 (2012).
[52] Z.-L. Xiang, S. Ashhab, J. Q. You, and F. Nori, Rev. Mod. Phys. **85**, 623 (2013).
[53] A. Stockklauser, P. Scarlino, J. V. Koski, S. Gasparinetti, C. K. Andersen, C. Reichl, W. Wegscheider, T. Ihn, K. Ensslin, and A. Wallraff, Phys. Rev. X **7**, 011030 (2017).
[54] G. Burkard, M. J. Gullans, X. Mi, and J. R. Petta, Nat. Rev. Phys. **2**, 129 (2020).
[55] G.-W. Deng, N. Xu, and W.-J. Li, *Quantum Dot Optoelectronic Devices* (Springer, Cham, Switzerland, 2020), pp. 107–133.
[56] R. J. Schoelkopf, P. Wahlgren, A. A. Kozhevnikov, P. Delsing, and D. E. Prober, Science **280**, 1238 (1998).
[57] W. Lu, Z. Ji, L. Pfeiffer, K. W. West, and A. J. Rimberg, Nature (London) **423**, 422 (2003).

[58] T. Fujisawa, T. Hayashi, Y. Hirayama, H. D. Cheong, and Y. H. Jeong, Appl. Phys. Lett. **84**, 2343 (2004).
[59] J. Bylander, T. Duty, and P. Delsing, Nature (London) **434**, 361 (2005).
[60] T. M. Buehler, D. J. Reilly, R. P. Starrett, A. D. Greentree, A. R. Hamilton, A. S. Dzurak, and R. G. Clark, Appl. Phys. Lett. **86**, 143117 (2005).
[61] C. Barthel, M. Kjærgaard, J. Medford, M. Stopa, C. M. Marcus, M. P. Hanson, and A. C. Gossard, Phys. Rev. B **81**, 161308(R) (2010).
[62] V. F. Maisi, O.-P. Saira, Yu. A. Pashkin, J. S. Tsai, D. V. Averin, and J. P. Pekola, Phys. Rev. Lett. **106**, 217003 (2011).
[63] M. Field, C. G. Smith, M. Pepper, D. A. Ritchie, J. E. F. Frost, G. A. C. Jones, and D. G. Hasko, Phys. Rev. Lett. **70**, 1311 (1993).
[64] J. M. Elzerman, R. Hanson, J. S. Greidanus, L. H. Willems van Beveren, S. De Franceschi, L. M. K. Vandersypen, S. Tarucha, and L. P. Kouwenhoven, Phys. Rev. B **67**, 161308(R) (2003).
[65] J. M. Elzerman, R. Hanson, L. H. Willems van Beveren, B. Witkamp, L. M. K. Vandersypen, and L. P. Kouwenhoven, Nature (London) **430**, 431 (2004).
[66] T. Ihn, S. Gustavsson, U. Gasser, B. Küng, T. Müller, R. Schleser, M. Sigrist, I. Shorubalko, R. Leturcq, and K. Ensslin, Solid State Commun. **149**, 1419 (2009).
[67] C. Barthel, D. J. Reilly, C. M. Marcus, M. P. Hanson, and A. C. Gossard, Phys. Rev. Lett. **103**, 160503 (2009).
[68] M. Zgirski, L. Bretheau, Q. Le Masne, H. Pothier, D. Esteve, and C. Urbina, Phys. Rev. Lett. **106**, 257003 (2011).
[69] C. Janvier, L. Tosi, L. Bretheau, Ç. Ö. Girit, M. Stern, P. Bertet, P. Joyez, D. Vion, D. Esteve, M. F. Goffman, H. Pothier, and C. Urbina, Science **349**, 1199 (2015).
[70] A. P. Higginbotham, S. M. Albrecht, G. Kiršanskas, W. Chang, F. Kuemmeth, P. Krogstrup, T. S. Jespersen, J. Nygård, K. Flensberg, and C. M. Marcus, Nat. Phys. **11**, 1017 (2015).
[71] M. Hays, G. de Lange, K. Serniak, D. J. van Woerkom, D. Bouman, P. Krogstrup, J. Nygård, A. Geresdi, and M. H. Devoret, Phys. Rev. Lett. **121**, 047001 (2018).
[72] T. Karzig, W. S. Cole, and D. I. Pikulin, Phys. Rev. Lett. **126**, 057702 (2021).
[73] J. J. Wesdorp, L. Grünhaupt, A. Vaartjes, M. Pita-Vidal, A. Bargerbos, L. J. Splitthoff, P. Krogstrup, B. van Heck, and G. de Lange, arXiv:2112.01936.
[74] D. Razmadze, D. Sabonis, F. K. Malinowski, G. C. Ménard, S. Pauka, H. Nguyen, D. M. T. van Zanten, E. C. T. O'Farrell, J. Suter, P. Krogstrup, F. Kuemmeth, and C. M. Marcus, Phys. Rev. Appl. **11**, 064011 (2019).
[75] G. Kiršanskas, M. Franckié, and A. Wacker, Phys. Rev. B **97**, 035432 (2018).
[76] F. Nathan and M. S. Rudner, Phys. Rev. B **102**, 115109 (2020).
[77] K. Mølmer, Y. Castin, and J. Dalibard, J. Opt. Soc. Am. B **10**, 524 (1993).
[78] M. B. Plenio and P. L. Knight, Rev. Mod. Phys. **70**, 101 (1998).
[79] A. J. Daley, Adv. Phys. **63**, 77 (2014).
[80] See Supplemental Material at http://link.aps.org/supplemental/10.1103/PhysRevB.107.L121401 for details about the quantum jump approach, derivations underlying our claims regarding parity insensitivity and parity blockade, and for additional data showing how the system parameters influence the Majorana signature.
[81] V. Derakhshan Maman, M. F. Gonzalez-Zalba, and A. Pályi, Phys. Rev. Appl. **14**, 064024 (2020).
[82] R. M. Lutchyn, J. D. Sau, and S. Das Sarma, Phys. Rev. Lett. **105**, 077001 (2010).
[83] Y. Oreg, G. Refael, and F. von Oppen, Phys. Rev. Lett. **105**, 177002 (2010).
[84] D. Sticlet, C. Bena, and P. Simon, Phys. Rev. Lett. **108**, 096802 (2012).
[85] M. Kjaergaard, K. Wölms, and K. Flensberg, Phys. Rev. B **85**, 020503(R) (2012).
[86] A.-P. Jauho, N. S. Wingreen, and Y. Meir, Phys. Rev. B **50**, 5528 (1994).
[87] D. J. Clarke, Phys. Rev. B **96**, 201109(R) (2017).
[88] E. Prada, R. Aguado, and P. San-Jose, Phys. Rev. B **96**, 085418 (2017).
[89] C. Knapp, T. Karzig, R. M. Lutchyn, and C. Nayak, Phys. Rev. B **97**, 125404 (2018).
[90] R. V. Mishmash, B. Bauer, F. von Oppen, and J. Alicea, Phys. Rev. B **101**, 075404 (2020).
[91] A. Khindanov, D. Pikulin, and T. Karzig, SciPost Phys. **10**, 127 (2021).
[92] M. Leijnse and K. Flensberg, Phys. Rev. B **86**, 134528 (2012).
[93] T. Dvir, G. Wang, N. van Loo, C.-X. Liu, G. P. Mazur, A. Bordin, S. L. D. t. Haaf, J.-Y. Wang, D. van Driel, F. Zatelli, X. Li, F. K. Malinowski, S. Gazibegovic, G. Badawy, E. P. A. M. Bakkers, M. Wimmer, and L. P. Kouwenhoven, Nature **614**, 445 (2023).
[94] M. Nitsch, R. Seoane Souto, and M. Leijnse, Phys. Rev. B **106**, L201305 (2022).